Carbon-Based Silicon Nanohybrid Anode Materials for Rechargeable Lithium ion Batteries

Hansinee Sitinamaluwa[1], Shanqing Zhang[2], Wijitha Senadeera[1], Geoffrey Will[1], Cheng Yan[1*]

[1]School of Chemistry, Physics and Mechanical Engineering, Queensland University of Technology, Brisbane QLD 4001, Australia.

[2]Centre for Clean Environment and Energy, Environmental Futures Research Institute and Griffith School of Environment, Gold Coast Campus, Griffith University, QLD 4222, Australia.

*Corresponding Author
c2.yan@qut.edu.au

Abstract

Silicon has demonstrated great potential as anode materials for next-generation high-energy density rechargeable lithium ion batteries. However, its poor mechanical integrity needs to be improved to achieve the required cycling stability. Nano-structured silicon has been used to prevent the mechanical failure caused by large volume expansion of silicon. Unfortunately, pristine silicon nanostructures still suffer from quick capacity decay due to several reasons, such as formation of solid electrolyte interphase, poor electrical contact and agglomeration of nanostructures. Recently, increasing attention has been paid to exploring the possibilities of hybridization with carbonaceous nanostructures to solve these problems. In this review, the recent advances in the design of carbon-silicon nanohybrid anodes and existing challenges for the development of high-performance lithium battery anodes are briefly discussed.

Keywords: Lithium ion battery, anode, nanohybrid, silicon, carbon

1. Introduction

Lithium ion battery is the energy storage device of choice for portable electronic devices and electric vehicles owing to its high energy density, lightweight and longer lifespan than other rechargeable battery technologies [1]. In the foreseeable future, electrification of transportation systems demands further improvements in battery technologies, particularly in energy density, rate capability and cycle life [2, 3]. For lithium battery anode, further increase

of energy density requires novel high-capacity materials since the currently used graphite is reaching its theoretical limit (372 mAh g^{-1}) [4]. Recently, silicon has emerged as a promising anode material owing to its highest known theoretical capacity (~4200mAh g^{-1}) [5, 6]. As shown in Table 1, a silicon atom can store up to 4.4 lithium atoms, while six carbon atoms in graphite can hold only one lithium atom [7]. However, such enormous capacity of silicon comes with the expense of significant structural changes, which results in severe volume expansion (~300%), high stresses and large material deformation [8], and quick capacity decay [9].

Recently, nanostructured silicon such as silicon nanowires, nanoparticles and thin films has demonstrated robust lithiation behaviour when compared to bulk silicon [10-19]. The reason is, nano-sized materials can successfully withstand the large volume change of silicon, preventing structure failure [20, 21]. Another advantage of nanoscale silicon is the shorter Li-ion transport distances, which can enhance rate capability. However, several other challenges exist such as formation of solid electrolyte interphase (SEI), a passivation layer developed on silicon surface due to decomposition of electrolyte. Due to high surface area and volume change, continuous SEI formation leads to irreversible capacity loss during each electrochemical cycle [22]. In contrast, graphite-based anode materials undergo minor structural changes during lithiation, with only ~10% volume expansion [8]. Also, the SEI layer formed on graphite is rather stable due to minor structural changes, and can act as a protective layer to the electrode. Also, large deformation influences the electrical contact between silicon nanostructures and current collector [23, 24]. In addition, electrochemical sintering (agglomeration of individual silicon particles when pressed together due to volume expansion) of nanostructured silicon cause agglomeration of particles [25], which in turn results in rapid capacity decay. Therefore, these issues must be addressed to realize the great potential of silicon nanostructured as new anode materials.

Recently, hybridization of silicon with other materials is attracting increasing attention. For example, silicon nanohybrids with carbonaceous materials [26-31], conductive polymers [32, 33] and metals [34-36] have demonstrated enhanced cycling stability compared with pristine silicon nanostructures. As well known, carbon is a unique material with excellent electrical and mechanical properties, which may be used to enhance the structure integrity of silicon anodes, provide effective electrical contact and prevent SEI formation. Moreover, carbonaceous materials may provide additional lithium storage sites.

In this paper, recent advances of carbon based silicon nanohybrid anode materials are reviewed, with a focus on the electrochemical performance of these electrode materials and its dependence with electrode architectures. The existing challenges in the field and future research needs are also discussed.

Table 1: Comparison of different anode materials for lithium ion battery. Reprinted with permission from [7] Copyright © 2011 Elsevier.

Materials	Li	C	Si	Sn	Sb	Al	Mg	Bi
Density (gcm^{-3})	0.53	2.25	2.33	7.29	6.7	2.7	1.3	9.78
Lithiated Phase	Li	LiC_6	$Li_{4.4}Si$	$Li_{4.4}Sn$	Li_3Sb	LiAl	Li_3Mg	Li_3Bi
Theoretical Specific Capacity ($mAh\ g^{-1}$)	3862	372	4200	994	660	993	3350	385
Theoretical Charge Density ($mAhcm^{-3}$)	2047	837	9786	7246	4422	268	4355	3765
Volume Change(%)	100	12	320	260	200	96	100	215
Potential vs. Li(~V)	0	0.05	0.4	0.6	0.9	0.3	0.1	0.8

2. Electrode design and fabrication

In an attempt to prevent the capacity fade of silicon-based anodes, several forms of carbonaceous materials are used including graphene (Gr), reduced graphene oxide (rGO), carbon nanotubes (CNT), carbon nanofibres (CNF), amorphous carbon (a-C) and graphite. This section summarizes the design and fabrication of carbon-silicon nanohybrid electrodes and effect of carbonaceous materials on capacity enhancement.

2.1. Graphene (Gr)/reduced graphene oxide (rGO) based electrodes

Since its discovery in 2004 [37], graphene has demonstrated excellent properties in advanced functional materials for numerous applications [38-41]. It has been used in various aspects in rechargeable lithium ion batteries, including silicon-based hybrid anode materials [42]. In general, incorporation of graphene enhances electrochemical performance of Si anodes due to several reasons. Graphene's high electrical conductivity [43] facilitates electron transport, while its flexibility and high strength [44] provide mechanical support and buffer the volume expansion of Si. Also, defects and edges of graphene act as additional lithium storage sites [45] and facilitate Li-ion transport [46] in the anode, which improves the rate capability. Furthermore, graphene sheets isolate the silicon particles from electrolyte to prevent excessive SEI formation [47].

Table 2 shows a summary of several graphene/rGO-Si composites with enhanced electrochemical performance. Architecture of Si-Gr/rGO nanohybrids is mainly two types: (i) Si nanoparticles (SiNP) dispersed in 3D Gr/rGO network and (ii) Si-Gr/rGO multilayered thin film composites. When designing graphene-silicon nanoparticle anodes a few major challenges exist. One is how to achieve good dispersion of graphene and silicon to avoid re-stacking of graphene sheets or agglomeration of silicon. Due to the inert nature of graphene, it is difficult to achieve a good dispersion by simple mechanical mixing [48, 49]. If silicon nanoparticles are not well dispersed, they are subjected to electrochemical sintering during charge-discharge process and tend to agglomerate [50]. Yang et.al. [51] introduced aromatic linkers into SiNP through diazonium chemistry to covalently anchor silicon nanoparticles into graphene sheets. In contrast, Ye et.al. [52] used a non-covalent anchoring method to effectively disperse graphene and silicon, using the electrostatic attraction by introducing positive and negative charges into their individual dispersions. Prolonged mechanical milling has also proven to be beneficial to achieve a good dispersion of nanoparticles [53, 54].

Use of graphene oxide (GO) can give effective solution for the dispersion problem, via covalently anchoring silicon particles to the functional groups available in GO. GO easily disperses in water and other solvents [55, 56], enabling easy mechanical mixing followed by freeze drying [57-59] to achieve well-dispersed SiNP/GO structures. Further improvements of GO/Si dispersions are obtained via methods such as using polymeric surfactants [60], chemical functionalization of silicon nanoparticles [61, 62], using functionalized graphene oxide [63]. However, GO is a poor conductor, therefore thermal reduction of GO/Si

composites are generally carried out after dispersion to restore its conductivity [64]. This results in reduced graphene oxide (rGO)/Si composites, which can be readily used as Li-ion battery anodes.

Table 2: Summary of graphene/rGO-silicon hybrid electrodes. SiNP- silicon nanoparticles, Gr- Graphene, CR- Capacity retention relative to second cycle discharge capacity, ICL – First cycle irreversible capacity loss

Anode architecture	Method of dispersion /deposition	Cycling stability	ICL (%)	Size of silicon (nm)	Silicon loading (%)	Ref
Si-Gr alternative multilayers	E beam evaporation	~90% CR ~1600 mAh g^{-1} for 30 cycles	17	100	46.6	[71]
SiNP dispersed between Gr sheets	Electrostatic Attraction	>95% CR 803 mAh g^{-1} at 100 cycles			67.3	[52]
SiNP encapsulated in 3D Gr network	CVD	66% CR 1000 mAh g^{-1} at 150 cycles	35.5		81	[69]
a-Si nanoislands deposited in porous GO network	CVD	60% CR 1103 mAh g^{-1} for 1000 cycles	7.5	<10	82	[26]
SiNP-multilayer Gr composite	Sonication	984 mAh g^{-1} for 50 cycles	19.9			[48]
Si thin film	Electrophoretic	87.7% CR	28.1			[72]

deposited on Gr thin film	deposition/ RF magnetron sputtering	150 cycles				
SiNP dispersed in rGO matrix	Sonication and subsequent freeze drying, followed by thermal reduction	96% CR ~600 mAh g^{-1} at 200 cycles		50-70		[58]
SiNP/porous rGO composite	Steam etching of Si/rGO aerogel	1004 mAh g^{-1} after 100 cycles (59.78 CR)	51.5	<100	~50	[67]
SiNP sandwiched between rGO sheets	Sonication, freeze drying and thermal reduction	746 mAh g^{-1} after 160 cycles (63.8% CR)	~20	10-20	74	[59]
rolled up Si/rGO bilayer nanomembranes	E beam evaporation of Si, spin coating of rGO	571 mAh g^{-1} after 2000 cycles 3.3% capacity decay per 100 cycles	51	25		[28]
Graphene encapsulated, carbon coated SiNP	Surface grafting of PANI in SiNP, wrap in GO sheets by electrostatic attraction and subsequent pyrolizing	900 mAh g^{-1} after 300 cycles 76% CR	35.6	<50	66	[60]

SiNP dispersed on graphene sheets	magnesium thermal reduction of the in-situ generated SiO2 particles on graphene	1374 mAh g^{-1} over 120 cycles	38	5	82	[70]

Among the reported nanohybrids, the CVD deposited Si backboned porous graphene oxide electrode (Figure 1) presented by Ko *et al.*[26] showed much better cycling stability, with average capacity of 1103 mAh g^{-1} for 1000 cycles. This binder-free anode design has a silicon loading of 82%, responsible for the high energy density. This composite is featured by ultra-small Si islands (below 10 nm), which have superior resistance to cracking and shorter Li transport distances, leading to first cycle Coulombic efficiency of 92.5%. It also demonstrates good resistance to SEI formation, due to effective isolation of Si nanoparticles from the electrolyte by graphene sheets. However, the CVD technique is generally expensive for scalable fabrication of large electrodes for practical applications.

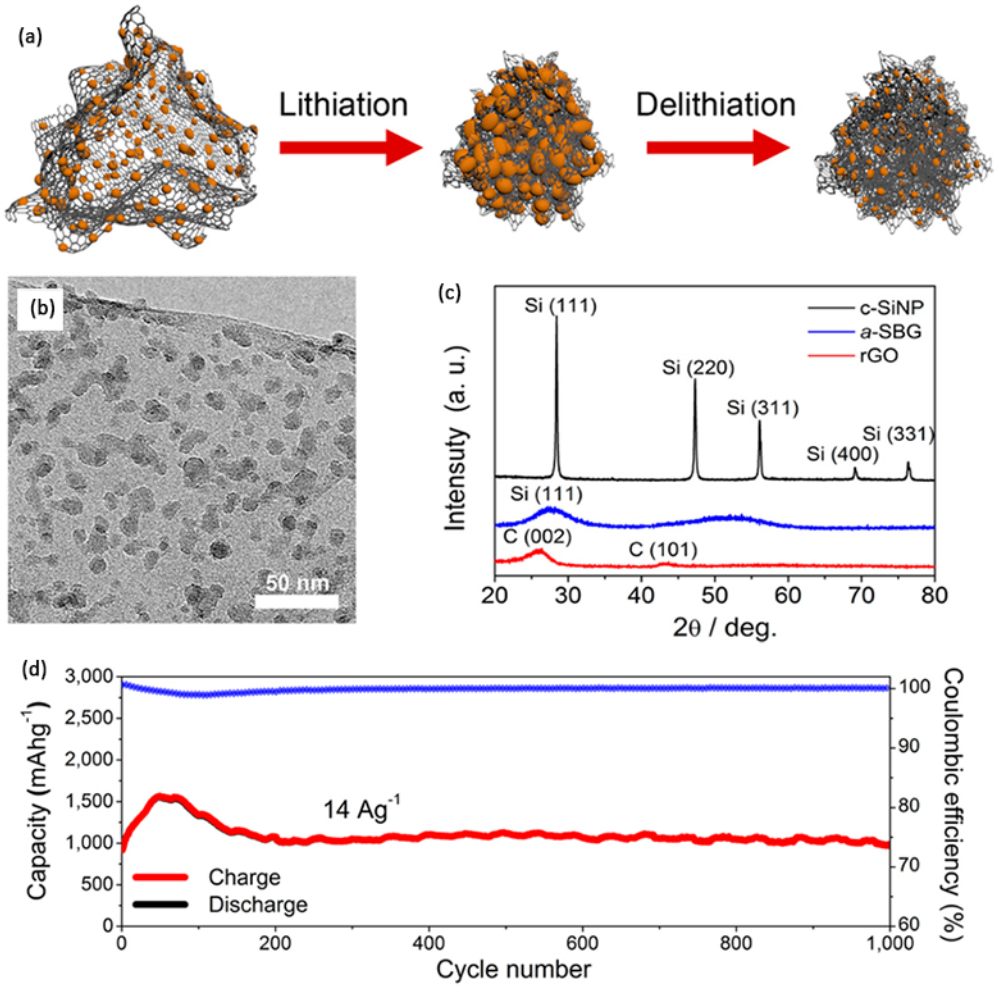

Figure 1: Si backboned graphene composite (a) Schematic design (b) TEM micrograph (c) XRD characterization of the electrode (d) cycling stability and Coulombic efficiency at 14A/g current rate. Reprinted with permission from [26] Copyright © 2014, American Chemical Society

Another advantage of SiNP-Gr/rGO composites is the ability to accommodate volume expansion, benefiting from the nanoporous / mesoporous structures [52, 53, 65-67]. However, it is difficult to tailor the pore distribution and the size of individual silicon particles in these composites. Therefore, though the total porosity is sufficient to accommodate ~300% volume expansion of silicon, local excessive expansion is expected. It was reported Si-Gr/rGO can be used to fabricate binder-free anodes, which in turn enable high silicon loading [68-70].

Silicon-graphene multilayered composites can provide effective buffering for volume expansion of silicon [28, 71]. Layered composites are generally fabricated using deposition

techniques such as sputtering, PVD or electron beam evaporation [28, 72]. In such composites graphene layers are incorporated between thin silicon layers to provide effective buffering for expansion while enhancing conductivity. Higher silicon layer thickness can cause cohesive cracking, while lower silicon layer thickness reduces the effective active material mass in the anode [10-12, 73]. Mori *et al*. [71] fabricated Si-graphene multilayer composite using electron beam evaporation, and concluded that most effective layer thickness is 100nm. One problem assisted with layered composites is absence of Li transport channels deeper into the composite. As Mori and co-workers point out in their study, when the layer number is increased Li cannot travel long enough to activate all Li-active sites. In their study, the 7-layered composite with 100-nm layer thickness showed the optimal performance, exhibiting 90% capacity retention up to 30 cycles with a capacity of ~1600 mAh g^{-1}.

Rolled-up Si-rGO membrane anodes (Figure 2) fabricated by Liu and co-workers[28] showed excellent cycling stability up to 2,000 cycles, with retained capacity of ~570 mAh g^{-1}. The Si/rGO bilayer was fabricated on a photoresist AR-P 3510 sacrificial layer. 25nm thick Si layer was deposited on photoresist layer using electron beam evaporation, and rGO suspension was spin coated on top of it. By selective etching of sacrificial layer, the rGO/Si membranes are naturally rolled up, forming a cylindrical void space in the middle. This void space provides strain relaxation, while the rGO layer acts as protective and conductive membrane. Also the 25nm thick silicon membrane is much resistant to cohesive cracking due to small (nano) size [10]. After 2,000 cycles, it exhibited a capacity of ~560 mAh g^{-1}, higher than the specific capacity of graphite. Also, the rate of capacity decay was lower as 3.3% per 100 cycles.

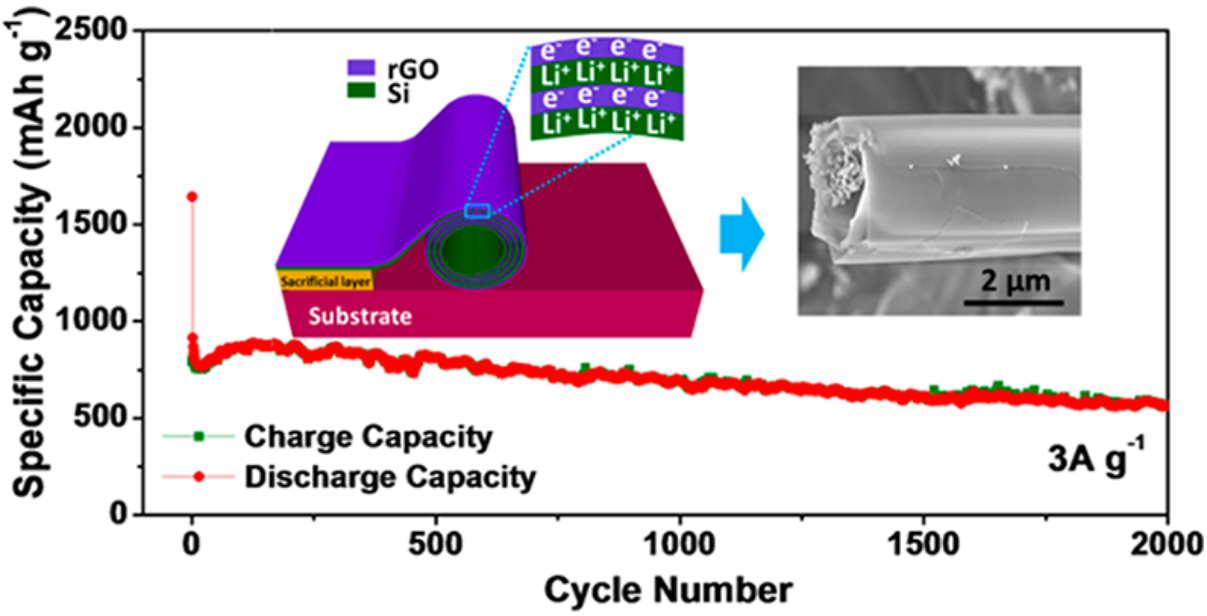

Figure 2: Anode architecture and cycling performance of rGO/Si rolled up nanomembranes. Reprinted with permission from [28] Copyright © 2015, American Chemical Society

In general, significant improvements have been achieved in terms of capacity when compared with theoretical limit of graphite (372 mAh g^{-1}), Table 2. However, first cycle irreversible capacity loss is significant, mainly attributed to formation of solid electrolyte interface. Further study is required to investigate the pore structure and how electrolyte interacts with the anode. Another problem is gradual capacity decay, which may have caused by continuous SEI formation and separation between silicon and graphene due to volume expansion of silicon. Also, the critical silicon particle size in carbonaceous matrices is unknown and has not been systematically investigated.

2.2. Amorphous carbon (a-C) based electrodes

SiNP/amorphous carbon electrodes are fabricated by dispersing silicon nanoparticles in carbon black [74, 75] or carbon precursor (E.g.: carbon containing polymers such as Polydopamine/PAN, or citric acid, coal tar pitch etc.) [76, 77], followed by thermal treatment such as annealing, pyrolizing or carbonization. Magnetron sputtering has been used to fabricate a-C/a-Si thin film multilayers [78, 79]. It has been reported carbon pre-coating of silicon particles can largely enhance performance of graphene/rGO based silicon electrodes [80-82]. Also, amorphous carbon provides effective electrical contact and Li ion transport, and acts as a buffer for volume expansion of silicon, significantly improving the

electrochemical performance of silicon nanostructures. Park and co-workers [75] used an ultrasonication based approach to disperse porous silicon nanoparticles in amorphous carbon matrix. Porous silicon nanoparticles were fabricated by selective etching of Ti-Si alloys, and mixed with carbon black (CB) using ultrasonication. Afterwards, annealing treatment resulted in highly dispersed SiNP in amorphous carbon. The anode showed about 83% capacity retention for 40 cycles. Chen and co-workers [74] used an emulsion based method, where SiNP (~50nm) are confined in a carbon black cage in an oil-based emulsion. After drying the emulsion, the SiNP remain in the spacious CB cages. They reported Initial capacity of 1540 mAh g^{-1}; however capacity retention after 50 cycles was only 66%. Wang *et al.* [77] prepared a mixture of coal tar pitch and SiNP, which is stable up to 1000 cycles. However, the silicon loading was only 20%, which resulted in only ~400 mAh g^{-1} average specific capacity. Wang et al. [76] fabricated amorphous carbon/SiO_x double layer coated silicon particles by carbonization of citric acid intruded silicon particles. Thin carbon layer enhanced the capacity, with 73% capacity retention (1450 mAh g^{-1}) after 100 cycles. Tong et al. [78] fabricated a-C/a-Si multilayered composites using magnetron sputtering. Relatively thick films (1.1μm) showed good cycling performance with a capacity of about 1,900 mAh g^{-1} at a current density of 2000 mAh g^{-1} over 200 cycles. Despite the enhancement of cycling stability, several drawbacks are identified in these electrode designs. High irreversible capacity of amorphous carbon causes significant capacity loss at the first cycle. Also, as demonstrated by Liu *et al.* [27], amorphous carbon layer might not be robust enough to withstand the high volume expansion of silicon, poor structural integrity and severe SEI formation.

Liu and co-workers presented a method to tune individual pore structures in amorphous carbon electrodes [29]. Firstly, they fabricated a yolk-shell type anode design where ~100nm silicon nanoparticles are encapsulated in a thin amorphous carbon shell, with a precisely tuned void space around each SiNP (Figure 3). The gap between silicon particle and carbon shell was controlled by using a SiO_2 sacrificial layer around SiNP, which was subsequently etched. This anode design exhibits high capacity (~2800 mAh g^{-1}initial, ~1500 mAh g^{-1} after 1000 cycles), enhanced capacity retention (74% after 1000 cycles) and high Coulombic efficiency (99.8%). In this anode design, the gap between SiNP and carbon shell played a critical role, which provided the space for expansion of silicon without disturbing the electrode structure.

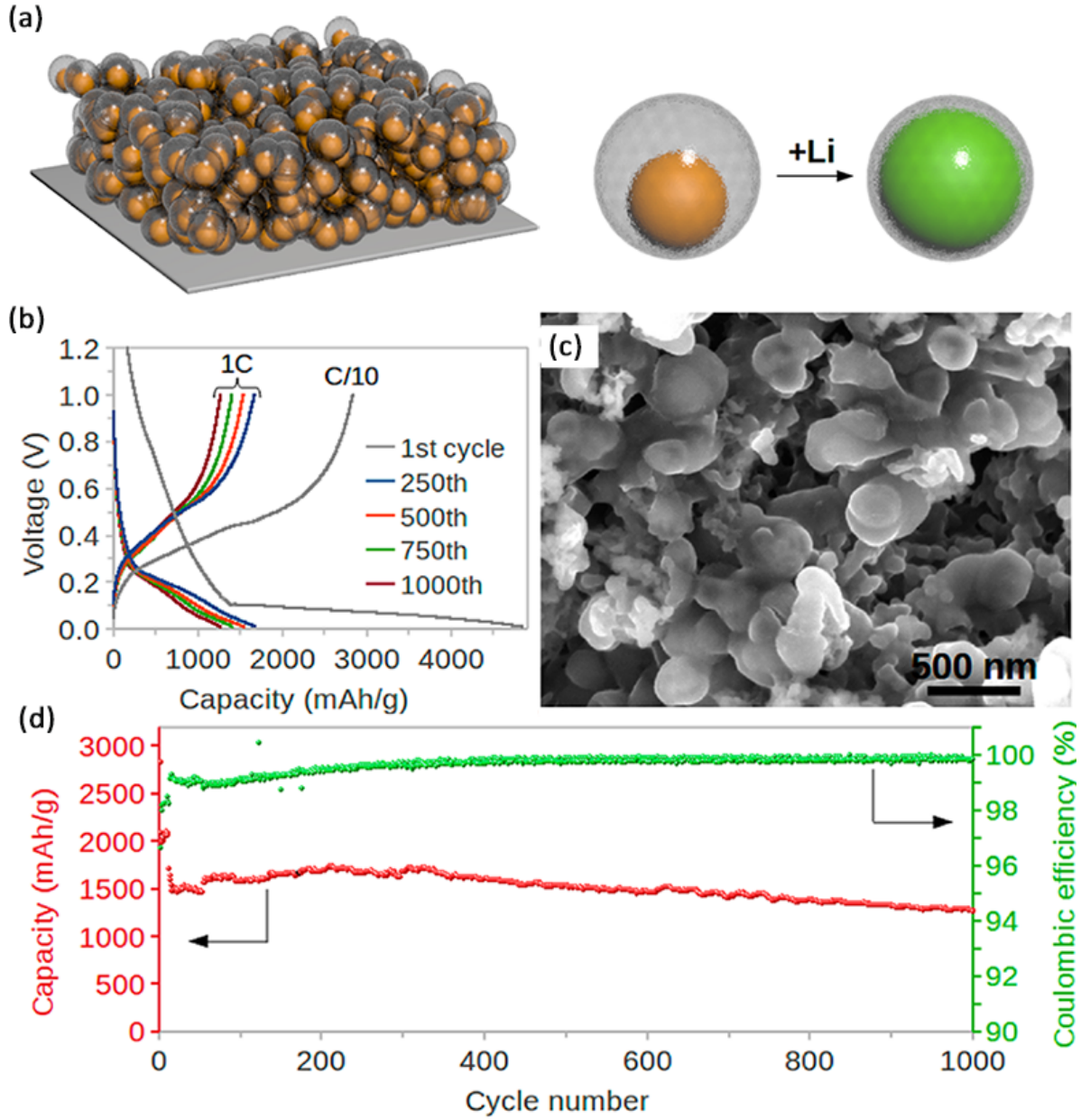

Figure 3: (a) design of Si-C Yolk-shell structures (b) Galvanostatic charge-discharge profiles of yolk-shell electrode (c) SEM micrograph of yolk-shell structure (d) Cycling stability and Coulombic efficiency of electrode. Reprinted with permission from [29] Copyrights © (2012) American Chemical Society

Next, Liu and co-workers further improved the earlier discussed yolk-shell design concept by introducing a hierarchical structure which was inspired by structure of pomegranate [27]

(Figure 4). In this design, single silicon nanoparticles are encapsulated in a conductive carbon shell, similar to yolk-shell structure, and an ensemble of the yolk-shell structures are encapsulated in a micron-size thicker carbon shell. This thicker carbon shell acts as a more-robust SEI barrier while providing a high electron and Li ion conductivity. The resulting pomegranate-like anode exhibits high areal capacity (1720 mAh cm^{-2}) after 1000 cycles, with 97% capacity retention with excellent Coulombic efficiency of 99.8%.

The recent advancements of amorphous carbon-silicon hybrid anodes are promising, however the high first cycle irreversible capacity loss is still an unsolved issue. For example, the yolk-shell structure showed ~40% irreversible capacity loss at first cycle. Liu *et al.* [27] demonstrated that, the first cycle capacity loss increases with carbon content in the anode, and the reason is attributed to the irreversible lithium trapping in amorphous carbon. This issue needs further attention, and as Liu and co-workers further point out, pre-lithiation of the electrode can be a feasible solution.

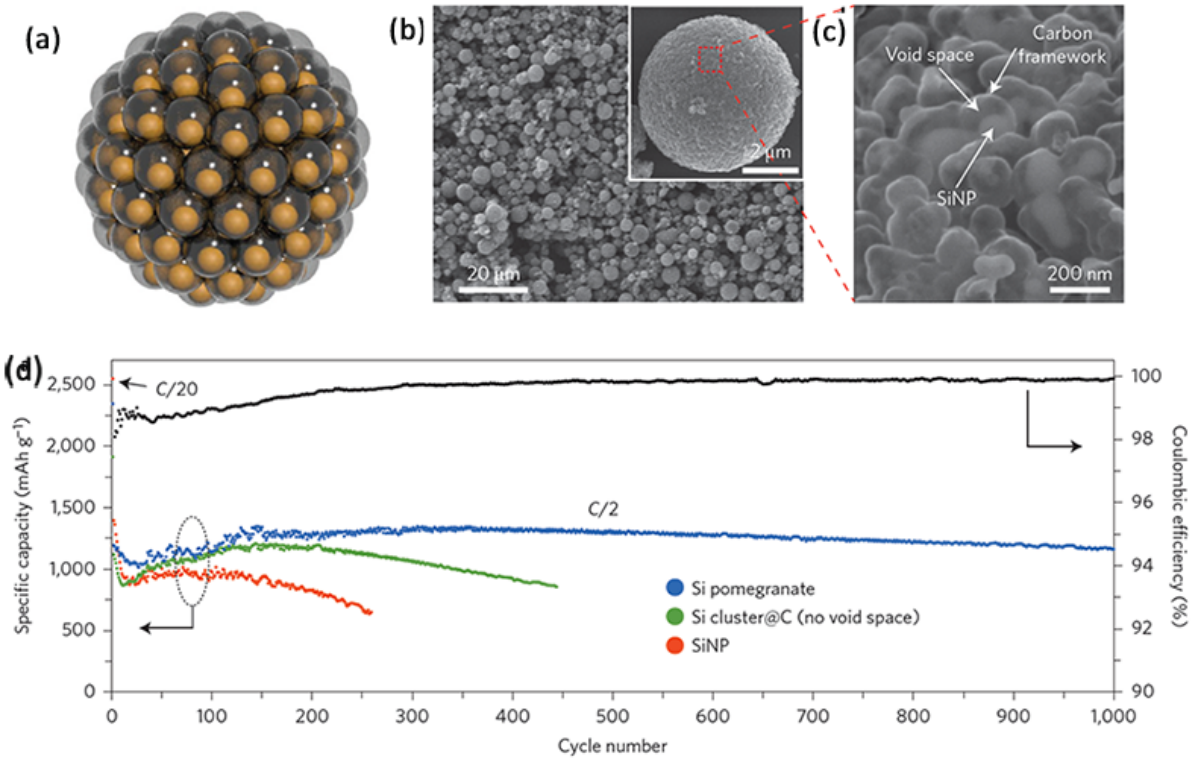

Figure 4: (a) Pomegranate inspired structure Si/a-C electrode design (b) SEM figure of spherical microbeads, which consist of an ensemble of Si/C yolk-shell structures (c) Enlarged view of a single microbead (d) Cycling stability of Si pomegranate structure, in comparison of Si/C structure with no void space and bear Si nanoparticles with no carbon addition.

2.3. Carbon nanofiber (CNF) based silicon nanohybrids

Electrospinning of carbon precursor and subsequent carbonization is a simple, cost effective and scalable method to fabricate carbon fibres [83]. Several techniques have been used to embed silicon active material into carbon fibre, which has proven to be high capacity and a better cycling stability. Gómez-cámer and co-workers [84] anchored silicon nanoparticles on carbon nanofibers by pyrolysis of resorcinol/formaldehyde polymer particles, and subsequent carbonization. It strongly fused the SiNP on CNF surface via SiO_x layer, which improved ion and electron conductivity. The composite showed initial capacity of ~2500 mAh g^{-1} and capacity retention of 500 mAh g^{-1} after 500 cycles. SiNP below 100 nm were robust in lithiation, however the main issues included severe SEI formation and irreversible capacity of SiO_x. Ji *et al.*[85] embedded silicon nanoparticles inside CNF, by electro-spinning Polyacrylonitrile/SiNP solution followed by carbonization (Figure 5a). However, the resulting composite showed relatively poor cycling stability as only 51% capacity remained from initial value at the 50^{th} cycle. Therefore, this method is not effective enough to prevent unstable SEI formation. Dirican *et al.* [86] used a CVD deposited amorphous carbon on SiNP embedded CNF to obtain a better cycling stability. However, agglomeration of SiNP has been a major issue and lead to quick capacity decay. Also absence of sufficient void spaced for expansion of silicon lead to fracture of carbon fibres [85]. Wang and co-workers [87] used electro-spinning to synthesize SiNP/porous CNF composite with improved cycling stability. The voids in porous carbon promoted strain relaxation in silicon and improved the cycling stability (about 870 mAh g^{-1}at 0.1 A/g after 100 cycles).

SiNP core-carbon shell nanofibers exhibit much more improved cycling stability, due to effective isolation of silicon particles from electrolyte, and hollow nanofiber provides additional space for Si expansion. Lee *et al.* [88] fabricated Si core-C shell nanofibers using co-axial electrospinning. In the core, a sacrificial material (Styrene-co-acrylonitrile) containing Si particles was used, and for the shell, PAN was used as carbonizing precursor. Average capacity of 590 mAh g^{-1} was obtained with only 8% degradation after 50 cycles. The hollow CNF structure provided effective strain relaxation for silicon nanoparticles. Hwang *et al.* [89] fabricated electrospun SiNP core- C shell nanofiber (Figure 5b), which exhibited

excellent cyclability for 300 cycles with retained capacity of 721 mAh g^{-1} and negligible capacity decay. Zhang *et al*. [90] reported a facile approach for mass production of SiNP core-carbon shell structures by a modified electrospinning method with subsequent calcination of carbon shells. The resulting composite could retain high capacity of 860 mAh $g^{-1}$for 200 cycles at a current rate of 0.3C. On the other hand, carbon core-Si shell nanowires have been also reported [56], where thin a-Si coating are deposited on CNF via chemical vapour deposition. Wang *et al*. [91] studied lithiation of amorphous silicon coated on CNF, and observed Li-Si reaction progress from a-Si surface and a-Si/CNF interface (Figure 5c). This observation further proves that carbon fibres can act as effective lithium ion carriers. However, longitudinal cracking of deposited a-Si was observed with electrochemical cycling.

Overall, Si-CNF hybrid electrode materials are very promising as lithium battery anodes with enhanced electrochemical performance. However the cycling stability should be improved further. Also the first cycle irreversible capacity loss is predominant, similar to other carbon based nanohybrids.

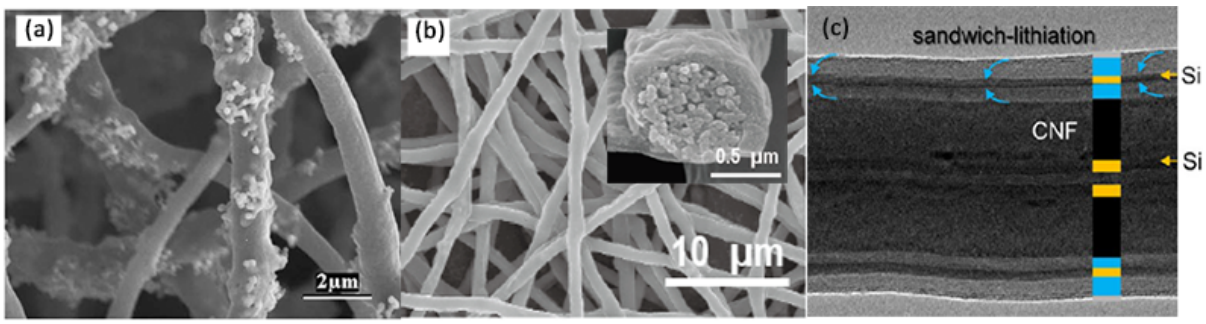

Figure 5: (a) SiNP embedded carbon nanofibers. Reprinted with permission from [85] Copyright © 2009 Elsevier Ltd (b) SiNP/CNF core-shell nanofibers. Reprinted with permission from [89] Copyright © 2012, American Chemical Society (c) Sandwich lithiation of a-Si thin layers deposited on carbon nanofibers. Reprinted with permission from [91] Copyright © 2012, American Chemical Society.

2.4. Graphite based silicon nanohybrids

Graphitic carbon has also been used to enhance capacity of silicon nanostructures. However, a ternary phase is also commonly used in such composites. For example, Chen *et al.* [92] used high energy ball milling to synthesize Si nanoparticle structure coated in B_4C and graphitic layer which showed excellent cyclability with ~822 mAh g^{-1}specific capacity after

100 cycles at 0.3C rate. Here B_4C particles act as a rigid skeleton to alleviate volume expansion of silicon. Gao *et al*. [93] synthesized a graphite based sandwiched nanostructure, where Si nanoparticles dip-coated on a nickel foam is covered by a graphite cloth. Enhanced electrochemical performance (1800 mAh g^{-1} at 2A/g after 500 cycles) was observed due to several reasons. Firstly, Ni welds the silicon active particles into Ni foam providing stable structure and the voids in Ni foam accommodate Si volume expansion. Secondly, graphite cloth provides fast electron and Li ion transport while acting as a barrier to SEI formation on active particles. Zhang *et al*. [94] used cobalt nanoparticles to improve electrochemical performance of silicon nanoparticle-graphite electrodes. Cho *et al*. [95] used nitrogen doped graphite with silicon nanowires, and they found increased charge capacity with N doping. The reason is believed as large Li storage capacity through dangling bonds in doped graphite structures.

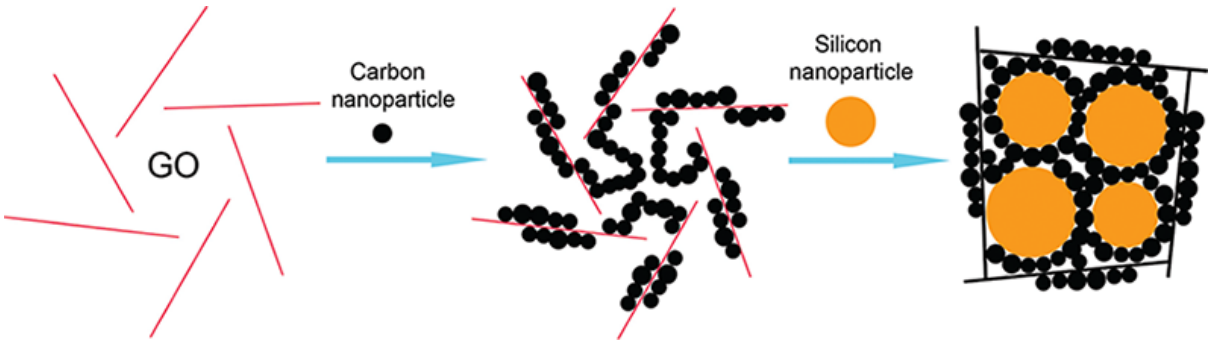

Figure 6: Carbon based multiphase composite made of Silicon nanoparticles, Carbon nanoparticles and Graphene. Reprinted with permission from [23] Copyright © 2012, American Chemical Society.

2.5. Composites of silicon with two or more types of carbonaceous materials

Carbon-based multiphase composites consisting of different carbonaceous materials have been reported. For example, carbon coated of silicon nanoparticles are embedded in graphene [80-82] or CNF [96]. Wu *et al.* [97] incorporated SiNP in a porous carbon layer composed of N-doped C framework, CB and CNT. This structure is further sandwiched by graphene sheets and a maximum reversible capacity of 1020 mAh g^{-1} and 75% capacity retention was achieved after 100 cycles. Also, Wang *et al.* [98] fabricated a Silicon nanowire/graphene/CNT network structure where CNT is mechanically binding silicon nanowires while graphene acting as a protective layer.

In another study by Hwang and Choi [99] a Si-Cu Quantum dot/graphene layer structure was fabricated using electrophotoresis, and a Cu_3Si interlayer was formed via subsequent annealing. The Cu_3Si interlayer exhibited a dual functionality as conductive and buffer layers. Further, Li-active CuO phase is also formed in connection with Cu_3Si, provided additional active vacancy sites for Li ion migration. Further, the layer structure is binder-free, with increased gravimetric anode capacity. Zhou et al. [24] reported a Si/Carbon nanoparticle/graphene structure prepared by simple mixing of SiNP/GO/Carbon nanoparticle followed by thermal reduction (Figure 6). In this composite, carbon nanoparticles could effectively connect SiNP to conductive network, while graphene sheets improved structural integrity. The resulting composite showed ca. 1521 mAh g^{-1} capacity at 0.2C over 200 cycles.

2.6. Effects of carbonaceous materials on capacity enhancement

As above, it is clear that the capacity enhancement by carbonaceous materials mainly depends on the electrode architecture. In general, the enhancement of electrochemical performance can be attributed to the following reasons.

(i) Increased electron and ion conduction paths into silicon active materials:

Electrochemical reaction inside a silicon anode in lithium battery can be described by

$$Si + xLi^+ + xe^- \rightarrow Li_xSi \qquad (1)$$

To achieve an acceptable rate, silicon active materials should be electrically connected to current collector and Li ions have to transport to the active material surface at a sufficient rate. Carbon based materials are superior conductors, thus the 3D conductive network formed by carbonaceous phase provide the effective electrical contact between current collector and silicon particles, even without the conductive binder. Also, carbon based materials can intercalate Li ions [42, 45, 100], thus they can transport Li ions effectively inside the anode. Therefore Li ions can be effectively transported to the active material without electrolyte/active material contact. Furthermore, the carbonaceous matrix provides additional lithiation capacity to the anode, which in turn increases the energy density.

(ii) Buffering volume expansion of silicon and maintaining structural integrity:

High volume expansion of silicon leads to structural changes in the anode, which can lead to electrical isolation of active particles from the conductive network. The strong and flexible mechanical support provided by carbonaceous materials can maintain the structural integrity

of the conductive network. Also, the force exerted on the silicon from the surrounding carbon materials can buffer the expansion of silicon.

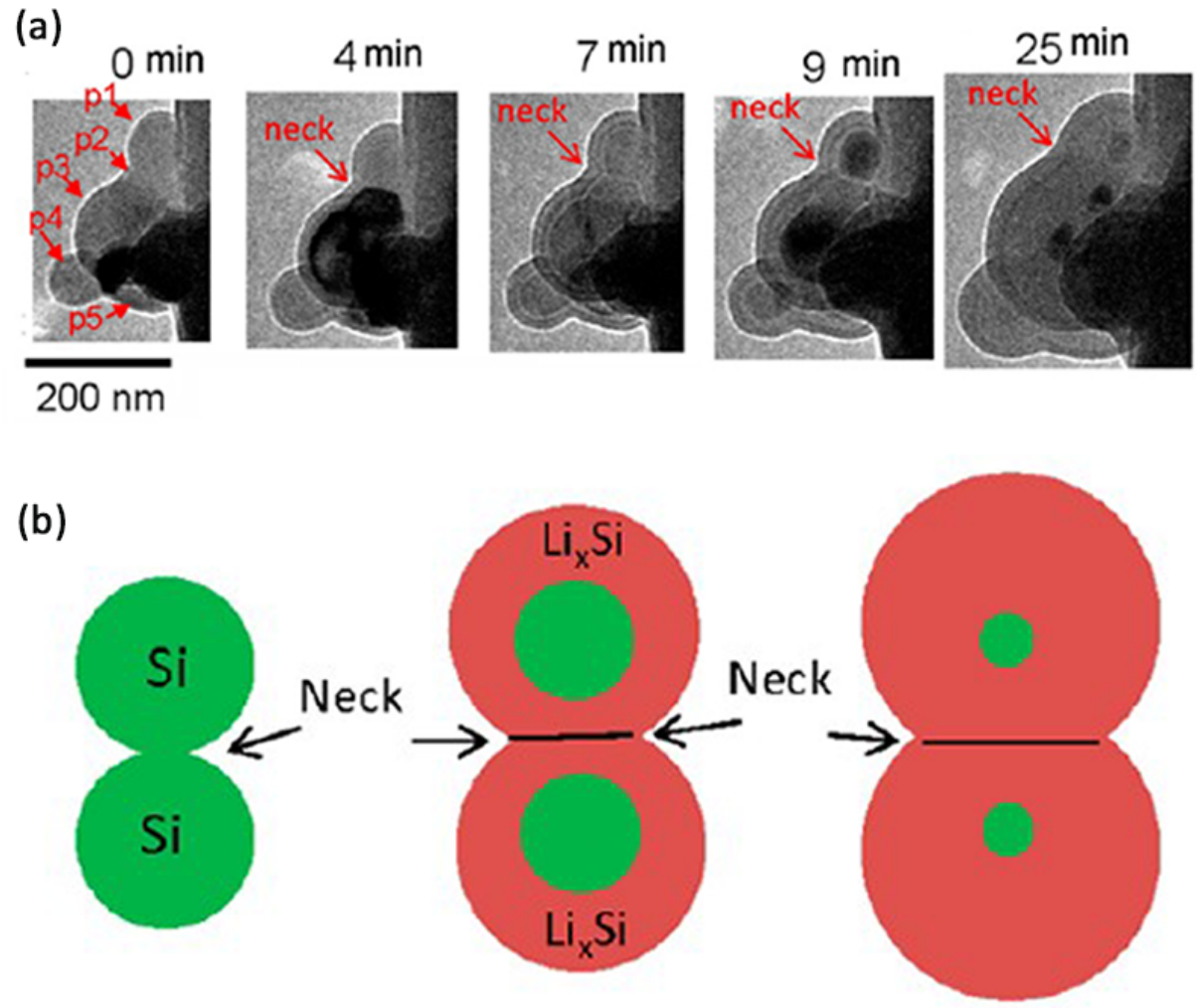

Figure 7: Lithiation induced neck flattening (a) In situ TEM observation of lithiation of carbon coated silicon particles (b) Illustration of lithiation induced contact flattening. Reprinted with permission from [101] Copyrights © (2012) American Chemical Society

(iii) Preventing contact between silicon active particles:

Agglomeration of silicon particles can happen in anodes due to electrochemical sintering [25, 50, 101], Figure 7. This can result in high stresses, longer Li conduction paths and electrical isolation, and quick capacity decay. Si-C layered composites inherently prevent the contact of silicon membranes; however, in Si nanoparticle composites special care has been taken to

prevent agglomeration. For example, covalent linkages are introduced to silicon particles to anchor silicon particles into graphene sheets, thereby preventing agglomeration [61, 102].

(iv) Preventing electrolyte-silicon contact to prevent unstable SEI formation:

A major reason for irreversible capacity of silicon is the formation of solid electrolyte interphase (SEI) due to decomposition of electrolyte on silicon surface [103]. High volume expansion of silicon makes this more significant as it continuously create fresh silicon surface [22]. Encapsulation of silicon in carbon based materials is an effective way to protect the silicon from SEI formation without affecting the electron and Li ion conductivity. The SEI on carbonaceous materials is a relatively stable and protective, which does not deteriorate battery performance [104].

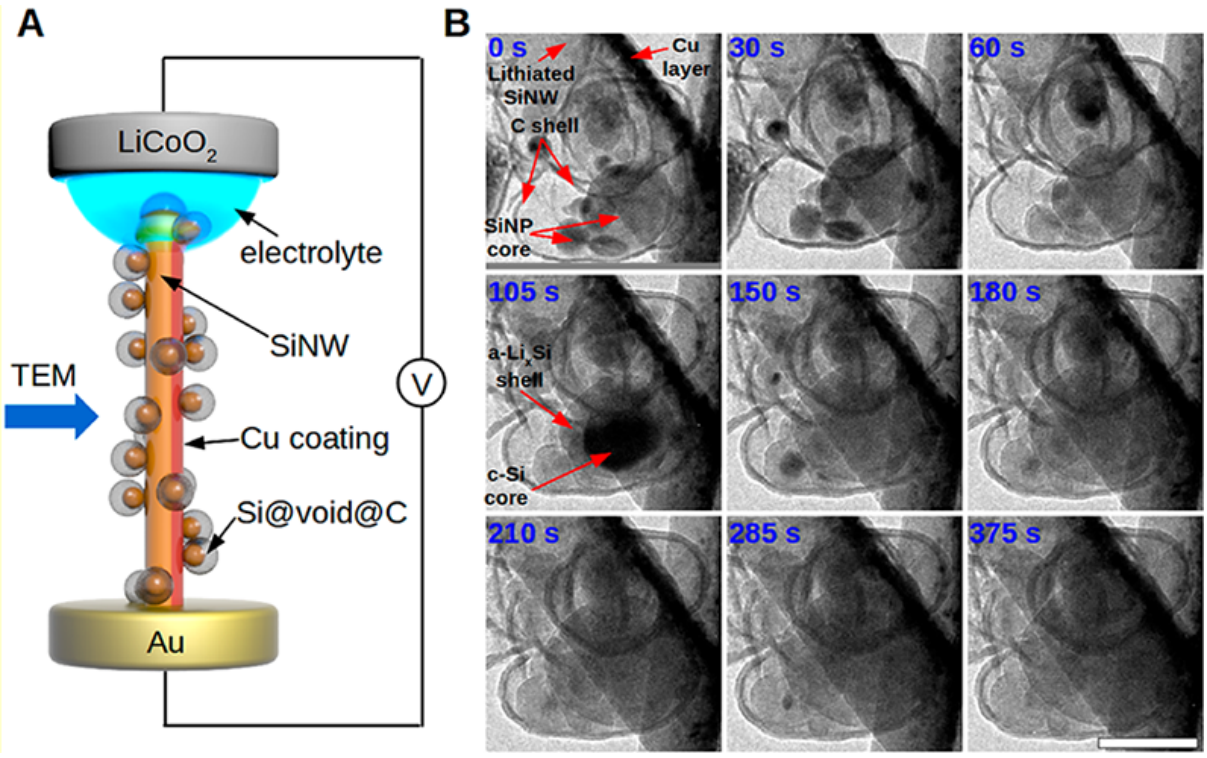

Figure 8: In situ TEM observation of lithiation behavior of silicon-carbon yolk-shell structures. (a) Schematic diagram of in situ TEM nano battery device (b) In sit TEM lithiation of silicon particles, which clearly demonstrate that the expansion of silicon particles is accommodated in the void space in carbon shell, without changing the shape or rupturing the shell. Reprinted with permission from [29] Copyrights © (2012) American Chemical Society

(v) Introducing void spaces for strain relaxation:

The well-known volume change in silicon upon complete lithiation is estimated to be ~300% [105], which can electrical disconnection between silicon and carbonaceous matrix. Introducing void spaces around silicon has been proven to be a much effective way to accommodate the expansion. For example, porous structures designed with silicon nanoparticles encapsulated by amorphous carbon can reduce lithiation induced strains [29], Figure 8.

(vi) Possibility of fabricating binder-free anodes:

For the active materials in powder form, such as silicon nanoparticles, the anode is fabricated by slurry coating of a mix of active particles such as carbon black and conductive polymeric binder such as PVDF, where the active particle loading is kept about 20% slurry weight. In this case, a large portion of anode is occupied with the binder which does not contribute to the capacity. In contrast, binder free anode architectures such as carbon based nanohybrids enables higher Si particle loading. For example, silicon loading over 80% is achieved using graphene-silicon nanohybrids [26, 69]

3. Electrochemical performance of carbon-silicon nanohybrid anodes

Most of the reported electrode designs show initial discharge capacity between 1000 mAh g^{-1} 3500 mAh g^{-1}, as shown in table 3. This is a significant improvement when compared with theoretical limit of graphite, which is only 372 mAh g^{-1}. It should be noted that not only silicon, but also the carbon phase contributes to the capacity of the electrode [100]. Also, carbon based nanostructures exhibit enhanced cycling stability when compared to pristine silicon nanostructures. For example, silicon nanowires directly grown on the current collector can deliver initial cycle capacity of 4,277 mAh g^{-1}, but has with very limited cycle life [13]. In contrast, carbon-silicon nanohybrids can deliver capacity values lower than pristine silicon but much higher than that of graphite, with prolonged cyclability. Several silicon-carbon nanohybrids have reported to be stable after 1000 cycles [26-29].

Despite these significant improvements, there are still a few challenges. One major problem is irreversible lithiation, which is mainly attributed to solid electrolyte interface formation[103, 106]. Irreversible lithiation is prominent during the first cycle, especially for nano scale materials with high surface area. Comparing initial Coulombic efficiency (CE) gained for different systems (Table 3), it is clear that first cycle irreversible capacity loss can get high up to 50% of the initial discharge capacity. It is not suitable for practical applications

since it can reduce overall lithiation capacity by consuming already limited lithium supply from the cathode. Initial CE higher than 90% has rarely been reported. Also, it is evident that the irreversible capacity loss is not highly dependent on carbon type. It is rather depending on the electrode design, and the extent to which the carbon phase actually encapsulates silicon nanostructures to supress the SEI formation.

It should be noted that the SEI formation on carbonaceous phase also participates in the irreversible capacity loss [106]. For example, Liu et al. [27] tested the same electrode architecture with 9% and 23% carbon, which delivered the initial Coulombic efficiency of 82% and 75%. Hence it is clear that only prevention of SEI formation on silicon is not sufficient. The irreversible capacity loss arise from carbonaceous phase also should be minimized. After few initial cycles, Coulombic efficiency generally is high as ~99%. On a different note, a completely opposite phenomenon was observed in some electrode designs, where there is a capacity gain in first few cycles [26, 52, 58, 63, 93, 99]. This is attributed to lithiation-induced structural changes for more active sites for lithiation.

Table 3: First cycle discharge capacity and Coulombic efficiency of different carbon based silicon composite electrodes.

Electrode materials	First cycle discharge capacity (mAh g-1)	First cycle Coulombic efficiency (%)	Reference
Si/Gr	2731	56	[69]
Si/Gr	2858	92.5	[26]
Si/Gr	2782	80.1	[48]
Si/Gr	2204	71.9	[72]
Si/rGO	2312	54	[58]
Si/rGO	1405	80	[59]
Si/rGO	2250	64.4	[62]
Si/rGO	1750	62	[70]
Si/a-C	2531	80	[79]
Si/a-C	2350	82	[27]

Si/CNF	967	53.9	[88]
Si/CNF	1327	71.1	[86]
Si/CNF	2320	88	[30]
Si/CNF	2071	71.7	[87]
Si/CNF	2314	60.2	[90]
Si/Graphite	2140	92	[95]
Si/Graphite	2900	71	[93]
Si/C/graphite	2959	64.7	[24]
Si/C/rGO	3877	48	[31]

Improvements achieved so far for cycle life and capacity maintenance is promising, however, in most of the composites gradual capacity decay occur during prolonged cycling. Apart from continuous solid electrolyte formation, other factors might contribute to capacity decay, such as electrical isolation of silicon particles due to the structural changes during volume expansion. Up to now, the critical size of silicon nanostructures in carbonaceous network has not been well identified. Also, the reported critical sizes reported for different silicon structures are quite different. For example, ~300nm for silicon nanowire [20], ~150nm for crystalline silicon nanoparticle [107], 870 nm for a-Si nanospheres [105] and 2.3μm for amorphous silicon nanopillars [108] were reported. Kim *et al*. [109] demonstrated that silicon particles above 10nm showed volumetric growth after electrochemical cycling. Certainly, silicon particles in carbonaceous matrices might exhibit different behaviour with buffering effect of the matrix. Also it is recently demonstrated that amorphous silicon structures are much more mechanically robust in lithiation than its crystalline counterpart [76, 108, 110]. Overall, more research efforts are needed to understand the failure mechanisms and reasons behind the capacity decay over cycling. However, failure analysis of the carbon-silicon nanohybrid materials is challenging due to the complexity of the structures.

Another major issue is low rate capability of these hybrid electrodes. Most of the claims on longer cycle lives are based on lower current rates less than 200mA/g. Figure 9 shows a comparison of rate capability of different electrode designs. It's clear that high charging rates lead to much lower lithiation capacity. Lithiation kinetics of silicon is another topic of

interest to lithium battery researchers. It has been recently reported lithium diffusion into silicon is the rate-limiting step for lithiation kinetics [105]. Therefore, the rate capability strongly depends on the Li ion diffusion distance into silicon active material. In principle, the rate capability can be improved when the size of silicon particles is reduced. Confirming that, the silicon/graphene hybrid reported by Ko et al. with silicon particle size <10 nm showed much higher rate capability exhibiting over 1000 mAh g^{-1} capacity at a much higher current rate of 28Ag^{-1} (ref -[26] in figure 9).

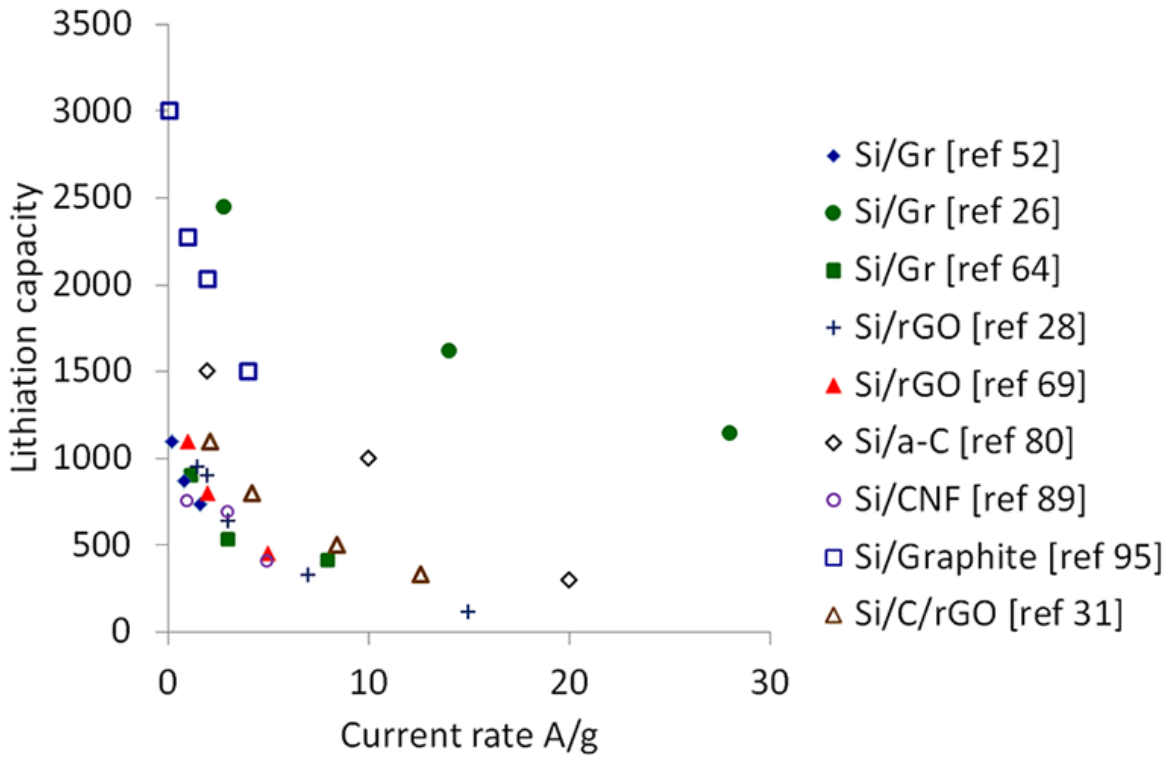

Figure 9: Capacity variation of Si-C nanohybrids at high current rates

Moreover, the capacity and the cycling stability greatly decrease with active material thickness. High active material loading is generally needed to achieve high energy density based on total weight and volume of the Li ion cell. Liu *et al*. [27] achieved stable cycling over 100 cycles for high active material mass loading of 3.12$mgcm^{-2}$. Certainly, further improvement in stable cyclability with high areal capacity is needed. In general, portable electronics require 80% capacity retention over at least 500 cycles, and for electrical vehicles the demands are much higher (at least 3000 stable cycles). Even though the current progress is promising, further improvements are required to meet these expectations.

Also, it should be noted that the cycling stability of these anodes is generally tested using a half-cell, with a Li foil as the counter electrode. However, its performance can be quite different as compared to a full cell. Even though these anodes show high gravimetric capacity, existing cathode materials are still not capable of matching this capacity [111]. Accordingly, extensive research has been carried out to improve the cathode materials but that is out of the scope of this review. To evaluate full cell performance of Si-graphene composite, Sun *et al*. [53] fabricated a Li-ion full cell using $LiMn_2O_4$ cathode which showed 600 mAh g^{-1}capacity retention over 30 cycles. They believed the poor performance can be attributed to the limited supply of Li ions from the low-capacity cathode.

4 Conclusions

Hybridization with carbonaceous materials such as graphene, reduced graphene oxide, amorphous carbon or graphite can greatly enhance electrochemical performance of nanostructured silicon anodes for lithium battery anodes. In such nanohybrids, carbonaceous phase provides not only effective electron and Li ion transport, but also mechanical support and buffer volume expansion of silicon. Most importantly, carbon based materials act as effective barrier to prevent the formation of unstable solid electrolyte interphase (SEI) on silicon. Electrochemical performance of these structures mainly depends on electrode structure. To design silicon-carbon nanohybrid anodes, the attention should be paid to realization of (i) mechanically robust silicon nanostructures, (ii) smallest possible Li ion diffusion paths in silicon nanostructures, (iii) mechanically robust electron and lithium ion transfer network which does not undergo disconnection due to volume expansion of silicon, (iv) 3D carbonaceous network to ensure all the silicon structures are actively participating in lithiation, (v) complete isolation of silicon active materials from the electrolyte to prevent SEI formation, (vi) tailored pore spaces around each individual silicon particles for strain relaxation, (vii) carbonaceous phase with minimal irreversible lithiation, and (viii) optimal silicon active particle loading. To this end, there are several technical problems to be solved. Firstly, simple, cost effective and scalable nano synthesis techniques are required to achieve well-controlled nanoscale electrode architectures. Secondly, more efforts are needed to minimize irreversible capacity loss caused by carbonaceous structure due to solid electrolyte interphase formation. Thirdly, a thorough understanding of lithiation kinetics in silicon active materials is needed to improve rate of lithiation in silicon nanostructures. Nevertheless, silicon-carbon nanohybrid anodes have demonstrated as promising approaches in development of next generation lithium battery systems.

Acknowledgement

Support from the ARC Discovery Project (DP150101717) is gratefully acknowledged. HS would like to acknowledge APA and IPRS scholarships provided by Queensland University of Technology.

References

[1] J.-M. Tarascon and M. Armand: Nature, 2001, 414, (6861), 359–367.

[2] M. S. Whittingham: Proc. IEEE, 2012, 100, (Special Centennial Issue), 1518–1534.

[3] E. Karden, S. Ploumen, B. Fricke, T. Miller and K. Snyder: J. Power Sources, 2007, 168, (1), 2–11.

[4] R. Marom, S. F. Amalraj, N. Leifer, D. Jacob and D. Aurbach: J. Mater. Chem., 2011, 21, (27), 9938–9954.

[5] K. E. Aifantis, S. A. Hackney and R. V. Kumar: 'High energy density

lithium batteries', 137–141; 2010, Weinheim: Wiley-VCH.

[6] G. Li, Z. Huang, Z. Zuo, Z. Zhang and H. Zhou: Mater Technol: Adv. Funct. Mater., 2014, 29, (A2), A77–A81.

[7] W.-J. Zhang: J. Power Sources, 2011, 196, (1), 13–24.

[8] A. Mukhopadhyay and B. W. Sheldon: Prog. Mater Sci., 2014, 63, 58–116.

[9] J. H. Ryu, J. W. Kim, Y. E. Sung and S. M. Oh: Electrochem. Solid-State Lett., 2004, 7, (10), A306–A309.

[10] S. Ohara, J. Suzuki, K. Sekine and T. Takamura: J. Power Sources, 2004,136, (2), 303–306.

[11] T. Takamura, S. Ohara, M. Uehara, J. Suzuki and K. Sekine: J. PowerSources, 2004, 129, (1), 96–100.

[12] T. Maruyama and H. Sudoh: J. Electrochem. Soc., 2001, 148, (12), G717–G720.

[13] C. K. Chan, H. Peng, G. Liu, K. McIlwarath, X. F. Zhang, R. A. Huggins and Y. Cui: Nat. Nanotechnol., 2008, 3, (1), 31–35.

[14] L.-F. Cui, R. Ruffo, C. K. Chan, H. Peng and Y. Cui: Nano Lett., 2009,9, (1), 491–495.

[15] H. Chen, J. Xu, P.-C. Chen, X. Fang, J. Qiu, Y. Fu and C. Zhou: ACS Nano., 2011, 5, (10), 8383–8390.

[16] H. T. Nguyen, F. Yao, M. R. Zamfir, C. Biswas, K. P. So, Y. H. Lee, S. M. Kim, S. N. Cha, J. M. Kim and D. Pribat: Adv. Energy Mater., 2011, 1, (6), 1154–1161.

[17] L. Hu, H. Wu, S. S. Hong, L. Cui, J. R. McDonough, S. Bohy and Y. Cui: Chem. Commun. (Camb), 2011, 47, (1), 367–369.

[18] S. Iwamura, H. Nishihara and T. Kyotani: J. Phys. Chem. C, 2012, 116, (10), 6004–6011.

[19] M. Wu, J. E. C. Sabisch, X. Song, A. M. Minor, V. S. Battaglia and G. Liu: Nano Lett., 2013, 13, (11), 5397–5402.

[20] I. Ryu, J. W. Choi, Y. Cui and W. D. Nix: J. Mech. Phys. Solids, 2011, 59, (9), 1717–1730.

[21] X. H. Liu, L. Zhong, S. Huang, S. X. Mao, T. Zhu and J. Y. Huang: ACS Nano, 2012, 6, (2), 1522–1531.

[22] J. H. Cho and S. T. Picraux: Nano Lett., 2014, 14, (6), 3088–3095.

[23] L.-F. Cui, L. Hu, H. Wu, J. W. Choi and Y. Cui: J. Electrochem. Soc., 2011, 158, (5), A592–A596.

[24] X. Zhou, Y. X. Yin, A. M. Cao, L. J. Wan and Y. G. Guo: ACS Appl. Mater. Interfaces, 2012, 4, (5), 2824–2828.

[25] K. Karki, E. Epstein, J. H. Cho, Z. Jia, T. Li, S. T. Picraux, C. Wang and J. Cumings: Nano Lett., 2012, 12, (3), 1392–1397.

[26] M. Ko, S. Chae, S. Jeong, P. Oh and J. Cho: ACS Nano, 2014, 8, (8), 8591–8599.

[27] N. Liu, Z. Lu, J. Zhao, M. T. McDowell, H.-W. Lee, W. Zhao and Y. Cui: Nat. Nanotechnol., 2014, 9, (3), 187–192.

[28] X. Liu, J. Zhang, W. Si, L. Xi, B. Eichler, C. Yan and O. G. Schmidt: ACS Nano, 2015, 9, (2), 1198–1205.

[29] N. Liu, H. Wu, M. T. McDowell, Y. Yao, C. Wang and Y. Cui: Nano Lett., 2012, 12, (6), 3315–3321.

[30] P.-C. Chen, J. Xu, H. Chen and C. Zhou: Nano Res., 2011, 4, (3), 290–296.

[31] B. Wang, X. Li, X. Zhang, B. Luo, M. Jin, M. Liang, S. A. Dayeh, S. Picraux and L. Zhi: ACS Nano, 2013, 7, (2), 1437–1445.

[32] H. Wu, G. Yu, L. Pan, N. Liu, M. T. McDowell, Z. Bao and Y. Cui: Nat. Commun., 2013, 4, 1943.

[33] G. Liu, S. Xun, N. Vukmirovic, X. Song, P. Olalde-Velasco, H. Zheng, V. S. Battaglia, L. Wang and W. Yang: Adv. Mater., 2011, 23, (40), 4679–4683.

[34] W. Si, X. Sun, X. Liu, L. Xi, Y. Jia, C. Yan and O. G. Schmidt: J. Power Sources, 2014, 267, 629–634.

[35] X. Huang, H. Pu, J. Chang, S. Cui, P. B. Hallac, J. Jiang, P. T. Hurley and J. Chen: ACS Appl. Mater. Interfaces, 2013, 5, (22), 11965–11970.

[36] F. F. Cao, J. W. Deng, S. Xin, H. X. Ji, O. G. Schmidt, L. J. Wan and Y. G. Guo: Adv. Mater., 2011, 23, (38), 4415–4420.

[37] K. S. Novoselov, A. K. Geim, S. Morozov, D. Jiang, Y. Zhang, S. A. Dubonos, I. Grigorieva and A. Firsov: Science, 2004, 306, (5696), 666–669.

[38] Y. Sun, Q. Wu and G. Shi: Energy Environ. Sci., 2011, 4, (4), 1113–1132.

[39] S. Stankovich, D. A. Dikin, G. H. Dommett, K. M. Kohlhaas, E. J. Zimney, E. A. Stach, R. D. Piner, S. T. Nguyen and R. S. Ruoff: Nature, 2006, 442, (7100), 282–286.

[40] V. Singh, D. Joung, L. Zhai, S. Das, S. I. Khondaker and S. Seal: Prog. Mater. Sci., 2011, 56, (8), 1178–1271.

[41] K. S. Novoselov, V. Fal, L. Colombo, P. Gellert, M. Schwab and K. Kim: Nature, 2012, 490, (7419), 192–200.

[42] M. Liang and L. Zhi: J. Mater. Chem., 2009, 19, (33), 5871–5878.

[43] Y. Zhang, Y.-W. Tan, H. L. Stormer and P. Kim: Nature, 2005, 438, (7065), 201–204.

[44] H. I. Rasool, C. Ophus, W. S. Klug, A. Zettl and J. K. Gimzewski: Nat. Commun., 2013, 4, 2811.

[45] Y. Liu, V. I. Artyukhov, M. Liu, A. R. Harutyunyan and B. I. Yakobson: J. Phys. Chem. Lett., 2013, 4, (10), 1737–1742.

[46] X. Zhao, C. M. Hayner, M. C. Kung and H. H. Kung: Adv. Energy Mater., 2011, 1, (6), 1079–1084.

[47] J. Luo, X. Zhao, J. Wu, H. D. Jang, H. H. Kung and J. Huang: J. Phys. Chem. Lett., 2012, 3, (13), 1824–1829.

[48] K. Eom, T. Joshi, A. Bordes, I. Do and T. F. Fuller: J. Power Sources, 2014, 249, 118–124.

[49] S.-L. Chou, J.-Z. Wang, M. Choucair, H.-K. Liu, J. A. Stride and S.-X. Dou: Electrochem. Commun., 2010, 12, (2), 303–306.

[50] P. Hovington, M. Dontigny, A. Guerfi, J. Trottier, M. Lagace, A. Mauger, C. M. Julien and K. Zaghib: J. Power Sources, 2014, 248, 457–464.

[51] S. Yang, G. Li, Q. Zhu and Q. Pan: J. Mater. Chem., 2012, 22, (8), 3420–3425.

[52] Y. S. Ye, X. L. Xie, J. Rick, F. C. Chang and B. J. Hwang: J. Power Sources, 2014, 247, 991–998.

[53] W. Sun, R. Hu, H. Liu, M. Zeng, L. Yang, H. Wang and M. Zhu: J. Power Sources, 2014, 268, 610–618.

[54] D. Chen, R. Yi, S. Chen, T. Xu, M. L. Gordin and D. Wang: Solid State Ionics, 2014, 254, 65–71.

[55] D. R. Dreyer, S. Park, C. W. Bielawski and R. S. Ruoff: Chem. Soc. Rev., 2010, 39, (1), 228–240.

[56] Y. Zhu, S. Murali, W. Cai, X. Li, J. W. Suk, J. R. Potts and R. S. Ruoff: Adv. Mater., 2010, 22, (35), 3906–3924.

[57] X. Zhou, Y.-X. Yin, L.-J. Wan and Y.-G. Guo: Chem. Commun., 2012, 48, (16), 2198–2200.

[58] V. Chabot, K. Feng, H. W. Park, F. M. Hassan, A. R. Elsayed, A. Yu, X. Xiao and Z. Chen: Electrochim. Acta, 2014, 130, 127–134.

[59] D. He, F. Bai, L. Li, L. Shen, H. H. Kung and N. Bao: Electrochim. Acta, 2015, 169, 409–415.

[60] X. Liu, Y. Du, L. Hu, X. Zhou, Y. Li, Z. Dai and J. Bao: J. Phys. Chem. C, 2015, 119, (11), 5848–5854.

[61] C. Sun, Y. Deng, L. Wan, X. Qin and G. Chen: ACS Appl. Mater. Interfaces, 2014, 6, (14), 11277–11285.

[62] Z.-F. Li, H. Zhang, Q. Liu, Y. Liu, L. Stanciu and J. Xie: ACS Appl. Mater. Interfaces, 2014, 6, (8), 5996–6002.

[63] F. Maroni, R. Raccichini, A. Birrozzi, G. Carbonari, R. Tossici, F. Croce, R. Marassi and F. Nobili: J. Power Sources, 2014, 269, 873–882.

[64] C. Gómez-Navarro, R. T. Weitz, A. M. Bittner, M. Scolari, A. Mews, M. Burghard and K. Kern: Nano Lett., 2007, 7, (11), 3499–3503.

[65] H. Tang, J. Zhang, Y. J. Zhang, Q. Q. Xiong, Y. Y. Tong, Y. Li, X. L. Wang, C. D. Gu and J. P. Tu: J. Power Sources, 2015, 286, 431–437.

[66] X. Gao, J. Li, Y. Xie, D. Guan and C. Yuan: ACS Appl. Mater. Interfaces, 2015, 7, (15), 7855–7862.

[67] X. Xin, X. Zhou, F. Wang, X. Yao, X. Xu, Y. Zhu and Z. Liu: J. Mater. Chem., 2012, 22, (16), 7724–7730.

[68] X. Zhou, A.-M. Cao, L.-J. Wan and Y.-G. Guo: Nano Res., 2012, 5, (12), 845–853.

[69] N. Li, S. Jin, Q. Liao, H. Cui and C. X. Wang: Nano Energy, 2014, 5, 105–115.

[70] Y. Du, G. Zhu, K. Wang, Y. Wang, C. Wang and Y. Xia: Electrochem. Commun., 2013, 36, 107–110.

[71] T. Mori, C.-J. Chen, T.-F. Hung, S. G. Mohamed, Y.-Q. Lin, H.-Z. Lin, J. C. Sung, S.-F. Hu and R.-S. Liu: Electrochim. Acta, 2015, 165, 166–172.

[72] Y. Q. Zhang, X. H. Xia, X. L. Wang, Y. J. Mai, S. J. Shi, Y. Y. Tang, L. Li and J. P. Tu: Electrochem. Commun., 2012, 23, 17–20.

[73] J. R. Szczech and S. Jin: Energy Environ. Sci., 2011, 4, (1), 56–72.

[74] Y. Chen, M. Nie, B. L. Lucht, A. Saha, P. R. Guduru and A. Bose: ACS Appl. Mater. Interfaces, 2014, 6, (7), 4678–4683.

[75] J.-B. Park, K.-H. Lee, Y.-J. Jeon, S.-H. Lim and S.-M. Lee: Electrochim. Acta, 2014, 133, 73–81.

[76] D. Wang, M. Gao, H. Pan, J. Wang and Y. Liu: J. Power Sources, 2014, 256, 190–199.

[77] Y.-X. Wang, S.-L. Chou, J. H. Kim, H.-K. Liu and S.-X. Dou: Electrochim. Acta, 2013, 93, 213–221.

[78] Y. Tong, Z. Xu, C. Liu, G. A. Zhang, J. Wang and Z. G. Wu: J. Power Sources, 2014, 247, 78–83.

[79] M. K. Datta, J. Maranchi, S. J. Chung, R. Epur, K. Kadakia, P. Jampani and P. N. Kumta: Electrochim. Acta, 2011, 56, (13), 4717–4723.

[80] Q. Yun, X. Qin, W. Lv, Y. B. He, B. Li, F. Kang and Q.-H. Yang: Carbon, 2015, 93, 59–67.

[81] R. C. de Guzman, J. Yang, M. M.-C. Cheng, S. O. Salley and K. Y. Simon: J. Power Sources, 2014, 246, 335–345.

[82] F. Zhang, X. Yang, Y. Xie, N. Yi, Y. Huang and Y. Chen: Carbon, 2015, 82, 161–167.

[83] A. Greiner and J. H. Wendorff: Angew. Chem. Int. Ed., 2007, 46, (30), 5670–5703.

[84] J. L. Gómez-Cámer, J. Morales and L. Sánchez: J. Mater. Chem., 2011, 21, (3), 811–818.

[85] L. Ji and X. Zhang: Carbon, 2009, 47, (14), 3219–3226.

[86] M. Dirican, O. Yildiz, Y. Lu, X. Fang, H. Jiang, H. Kizil and X. Zhang: Electrochim. Acta, 2015, 169, 52–60.

[87] M.-S. Wang, W.-L. Song, J. Wang and L.-Z. Fan: Carbon, 2015, 82, 337–345.

[88] B.-S. Lee, S.-B. Son, K.-M. Park, J.-H. Seo, S.-H. Lee, I.-S. Choi, K.-H.Oh and W.-R. Yu: J. Power Sources, 2012, 206, 267–273.

[89] T. H. Hwang, Y. M. Lee, B.-S. Kong, J.-S. Seo and J. W. Choi: Nano Lett., 2012, 12, (2), 802–807.

[90] C. Zhang, R. Yu, T. Zhou, Z. Chen, H. Liu and Z. Guo: Carbon, 2014, 72, 169–175.

[91] J. W. Wang, X. H. Liu, K. Zhao, A. Palmer, E. Patten, D. Burton, S. X. Mao, Z. Suo and J. Y. Huang: ACS Nano, 2012, 6, (10), 9158–9167.

[92] X. Chen, X. Li, F. Ding, W. Xu, J. Xiao, Y. Cao, P. Meduri, J. Liu, G. L. Graff and J. G. Zhang: Nano Lett., 2012, 12, (8), 4124–4130.

[93] C. Gao, H. Zhao, P. Lv, T. Zhang, Q. Xia and J. Wang: ACS Appl. Mater. Interfaces, 2015, 7, (3), 1693–1698.

[94] J. Zhang, Y. Liang, Q. Zhou, Y. Peng and H. Yang: J. Power Sources, 2015, 290, 71–79.

[95] Y. J. Cho, H. S. Kim, H. Im, Y. Myung, G. B. Jung, C. W. Lee, J. Park, M.-H. Park, J. Cho and H. S. Kang: J. Phys. Chem. C, 2011, 115, (19), 9451–9457.

[96] S. Y. Kim, K. S. Yang and B.-H. Kim: J. Power Sources, 2015, 273, 404–412.

[97] J. Wu, X. Qin, H. Zhang, Y.-B. He, B. Li, L. Ke, W. Lv, H. Du, Q.-H. Yang and F. Kang: Carbon, 2015, 84, 434–443.

[98] B. Wang, X. Li, B. Luo, X. Zhang, Y. Shang, A. Cao and L. Zhi: ACS Appl. Mater. Interfaces, 2013, 5, (14), 6467–6472.

[99] B. Rangasamy, J. Y. Hwang and W. Choi: Carbon, 2014, 77, 1065–1072.

[100] N. A. Kaskhedikar and J. Maier: Adv. Mater., 2009, 21, (25–26), 2664–2680.

[101] M. Gu, Y. Li, X. Li, S. Hu, X. Zhang, W. Xu, S. Thevuthasan, D. R. Baer, J. G. Zhang, J. Liu and C. Wang: ACS Nano, 2012, 6, (9), 8439–8447.

[102] G. Zhao, L. Zhang, Y. Meng, N. Zhang and K. Sun: J. Power Sources, 2013, 240, 212–218.

[103] M. Nie, D. P. Abraham, Y. Chen, A. Bose and B. L. Lucht: J. Phys. Chem. C, 2013, 117, (26), 13403–13412.

[104] V. A. Agubra and J. W. Fergus: J. Power Sources, 2014, 268, 153–162.

[105] M. T. McDowell, S. W. Lee, J. T. Harris, B. A. Korgel, C. Wang, W. D. Nix and Y. Cui: Nano Lett., 2013, 13, (2), 758–764.

[106] P. Verma, P. Maire and P. Novák: Electrochim. Acta, 2010, 55, (22), 6332–6341.

[107] X. H. Liu and J. Y. Huang: Energy Environ. Sci., 2011, 4, (10), 3844–3860.

[108] L. A. Berla, S. W. Lee, I. Ryu, Y. Cui and W. D. Nix: J. Power Sources, 2014, 258, 253–259.

[109] H. Kim, M. Seo, M. H. Park and J. Cho: Angew. Chem. Int. Ed., 2010, 49, (12), 2146–2149.

[110] B.-C. Yu, Y. Hwa, J.-H. Kim and H.-J. Sohn: J. Power Sources, 2014, 260, 174–179.

[111] B. Xu, D. Qian, Z. Wang and Y. S. Meng: Mater. Sci. Eng., R, 2012, 73, (5), 51–65.